

Analysis of the experimental results from the EAS installation GAMMA at Mt. Aragats

V.S. Eganov^(*), A.P. Garyaka^(*), E.V. Korkotian^(*),
E.A. Mamidjanian^(**), R.M. Martirosov^{1(*)}, J. Procureur^(***),
H.E. Sogoyan^(*), M.Z. Zazyan^(*)

(*) Yerevan Physics Institute, Br. Alikanian St.2, 375036 Yerevan, Republic of Armenia

(**) P.N. Lebedev Institute Leninsky pr. 56, Moscow 117924, Russia

(***) Centre d Etudes Nucleaires de Bordeaux-Gradignan, Université de Bordeaux 1
rue du Solarium, 33175 Gradignan-Cedex, France

December 2, 2024

Abstract

The phenomenological characteristics of the electron and muon components of EAS with the size $10^5 \leq N_e \leq 10^7$ are obtained by the GAMMA installation of the ANI experiment at the Mt. Aragats in Armenia at the observation level 700 g.cm^{-2} . The experimental results are compared with other experiments and with the simulation carried out using the CORSIKA code.

1 ¹Introduction

The particle physics and astrophysics aspects of air shower studies are closely interlaced. The problems of sources and nature of the primary radiation and features of the high energy hadron interactions cannot be solved separately. The history of attempts to clarify the origin of the appreciable change in the index of the shower size spectrum (the *knee*), which was found more than 40 years ago [1] and confirmed by other experiments, is the best manifestation of that. Many new experiments were born devoted to the observation of various

¹Corresponding author. E-mail: martir@lx2.yerphi.am

components of EAS, including Cherenkov light in the atmosphere and experiments under water. However, up to now there is no unequivocal explanation of the reason of this phenomena. The most popular interpretation of the *knee* is the existence of the *knee* in the primary cosmic ray energy spectrum at energy about $(3-5) \cdot 10^6$ GeV and, as a possible consequence, the change of the mass composition. There are different experimental analysis leading to opposite conclusions about primary composition after *knee* (lighter [2], normal [3][4] or heavier [5][6][7]).

At the same time there is an alternative explanation of the *knee*, also based on some inconsistencies in the EAS data, connected with a modification in the hadronic interaction properties [8][9] to the change of the number and energy spectrum of the secondaries. The complex installations, which measure electromagnetic component as well as muon and hadron components of EAS have the best opportunities to explore the nature of the *knee*. HADRON-2 [10] on Tien-Shan and KASCADE [11] are installations of such a kind. The hadron component data obtained from these installations show the fast absorption of the high energy hadrons, which is impossible to be explained by the energy increase of the interaction cross-section only. At the same time, the electromagnetic component data are in an agreement with the QGSJET model and correspond to the mixed composition of primary with progressive changing of the mass composition. In the work [9] on the bases of the Tien-Shan data analysis it is supposed that there is no *knee* in the primary spectrum and *knee* in the EAS size spectrum is explained by the change of the hadronic interaction in the atmosphere. This explanation is based on the results of the EAS electromagnetic component study [12], according to which there is no *knee* neither in the *young* showers spectrum (showers with $S < 0.75$, generated by primary protons interacted in the depth of atmosphere), nor in the *old* showers ($S > 1.05$) one. And the existence of the *knee* in the same spectra of other experiments could be explained by the missing of the young showers.

On the other hand it is not so clear situation with the so-called *reverse knee* in the EAS size spectrum at $N_e \sim (2 - 3) * 10^7$, which was discovered in [13]. Subsequently the same irregularity was obtained once again in Tien-Shan experiment [12].

At present, practically all experiments on research of the cosmic rays in the energy range 10^{14} - 10^{17} eV are pointed to investigate the nature of the *knee*. We have to point out that the KASCADE [11], CASA-MIA [14] and EAS-TOP [15] experiments present the basic advantage to have their data

analyzed using multiparameter procedures. Only such an approach to study the EAS characteristics allows some advance in understanding of the reasons of the existence of the *knee* in the spectrum on N_e . In this paper, we present the experimental results of the GAMMA installation of the experimental complex ANI also working in this field.

The GAMMA installation is located on hillside of the Mt. Aragats in Armenia (3200 m a.s.l.). In comparison with the other large scale experiments with the same goals, the high-altitude observation level of the GAMMA installation provides some advantages, in particular for minimizing the intrinsic fluctuations of the observables due to the stochastic character of the EAS development in atmosphere. This will add some new observations, which would clearly complement the data from KASCADE (near sea-level), CASA-MIA (1200 meters), and EAS-TOP (2000 meters). In the present work, showers are simulated using the CORSIKA code 5.20 [16] in which the hadronic interactions are described by the VENUS model,[17]. On the other hand, to compare the simulation data with experimental ones, the normal mixed composition was used, i.e. proton-40 %, α -21%, light-nuclei ($\langle A \rangle = 14$)-14%, medium-nuclei ($\langle A \rangle = 26$)-13% and heavy-nuclei ($\langle A \rangle = 56$)-12%

2 Present status of the GAMMA EAS installation

The GAMMA installation [18] was realized as a part of the project ANI [19] in an attempt to continue experimental study of the hadronic interactions and the energy spectrum and mass composition of the primary cosmic radiation in the energy range of $10^{14} - 10^{17}$ eV.

After some years spent to enlarge the effective area of the muon underground detector, which was necessary to elaborate methodical studies of the detector parameters, to investigate carefully the array response and to determine the precision of the shower parameter estimation, the GAMMA experiment is, now, effectively running.

GAMMA is a central type array and consists of two main parts (*figure 1*):

- (i) the surface part, for the registration of the EAS electromagnetic component;
- (ii) the large muon underground detector, to register the EAS muon component.

2.0.1 The surface scintillation array

The surface scintillation array consists of 25 groups of 3 scintillation detectors placed on concentric circles with radii of 17, 28, 50 and 70 m . Each of the detectors has 1 m^2 of effective area. They are distributed on the full area of $\approx 1.5 \cdot 10^4 m^2$. An additional station with 20 detectors of the same type is placed at the 135 m from the installation centre. The energy threshold for the registration of the electrons flux, $E_e^{thres} \simeq 9.5$ MeV, is estimated taking into account the thickness and the specificities of the detectors and registration stations. The calibration of detectors has been carried out by periodical (each hour) registration of the cosmic ray background particles. It was taken into account that the most probable value of the registered particles differs from 0⁰ and depends on the observation level [20].

Each of the 25 registration stations is equipped with the timing channel which allows to determine the angular coordinates of the shower axis. The trigger condition for one EAS registration is that in each of four groups of detectors placed at 17 meters from the array centre, two detectors have to register a flux density with $\rho \geq 3 \text{ part}/m^2$.

The main EAS parameters: coordinates and angles of the shower axis (X, Y, θ, φ) , number of electrons (N_e) and age parameter S_{NKG} are obtained using the SPACE code [21] created on the basis of the statistical methods for the solution of the inverse problem [22]. Taking into account the detector response, GAMMA array geometry and using Monte-Carlo procedure the data bank of pseudo experimental showers was created and treated by the same SPACE code.

As the result of this study, the following accuracies on the EAS parameter estimations are obtained: $\Delta X, \Delta Y \leq 3m$ (for $R \leq 40m$), $\sigma_\theta \simeq 1.5^\circ$, $\sigma_\varphi \simeq 8^\circ$, $\sigma_{N_e} / \langle N_e \rangle \leq 20\%$.

Furthermore, the analysis of the shower registration efficiency shows that the showers with particle number $N_e \gtrsim 3 \cdot 10^5$ within 20 m and $N_e \gtrsim 10^6$ within 40 m from the array centre are registered with 100% efficiency.

2.0.2 Underground muon detector

The layout of the muon underground detector is shown in *figure 2*. As for the GAMMA surface part identical scintillation detectors with $S = 1m^2$ were used for the registration of the EAS muon component. It should be noted that the muon scintillation detectors are divided into 2 groups placed

under different absorber thickness. This allows to study EAS muons with 2 different energy thresholds: $E_\mu \gtrsim 5 \text{ GeV}$ (Hall) and $E_\mu \gtrsim 2.5 \text{ GeV}$ (Tunnel). These thresholds were estimated experimentally using scintillation telescope with a small solid angle. The arrangement of the muon detectors gives the possibility to determine the muon lateral distribution up to $60m$ at $E_\mu \gtrsim 5 \text{ GeV}$ and up to $90m$ at $E_\mu \gtrsim 2.5 \text{ GeV}$.

Some peculiarities of the GAMMA array geometry make necessary to pay attention on the azimuth angle symmetry of data. The surface detectors are placed on the hillside and sometimes the difference between Z coordinates of the individual detectors is reaching $18m$. On the other hand, the position of muon detector is very asymmetric in regard to the geometric centre of our installation. In this case, the influence of azimuth angle φ could be strong. To check this effect we divided the observed showers into four groups with $\varphi \in [0 - 90]^\circ, [90 - 180]^\circ, [180 - 270]^\circ, [270 - 360]^\circ$. The comparison of the average muon lateral distributions for each of these groups by φ is shown in *figure 3 (a, b)* for $\langle N_e \rangle = 1.28 \cdot 10^6$. It can be visible, that the difference of the muon lateral distributions for the different ranges of φ is quite negligible. Furthermore, it is necessary to point out that for the small distances (less than $15m$ for $E_\mu \gtrsim 2.5 \text{ GeV}$ and $8m$ for $E_\mu \gtrsim 5 \text{ GeV}$) there is a significant influence of the punch through of particles (high energy electrons and hadrons) and these distances are excluded from the further analysis.

3 Results

We have used the experimental data obtained during 3300 hours operation time. The number of EAS with $N_e \geq 10^5$ and with zenith angle $\theta \leq 30^\circ$ is ~ 260.000 . The effective area for the selection of the EAS axis is $\sim 5.000m^2$.

3.1 Electromagnetic component characteristics

The main parameters of the EAS electromagnetic component at the given observation level are: the total number of the charge particles or shower size N_e and the lateral shower age parameter S . In order to obtain the EAS size spectrum and to investigate its behaviour in the *knee* region the correct estimation of these parameters is needed.

Usually in the energy region of $10^5 - 10^7$ GeV the scintillation detectors are used to register the EAS charged particles. However it is well known that such type of a detector registers not only the EAS charged particles, but also electrons generated in the absorber above as well as in the scintillator by EAS photons. This contribution to the measured charged particle density depends both on the scintillator thickness and the distance of detector from the shower axis.

The comparison of the charge particle densities seen by scintillation detectors and Geiger counters has been made for different distances from the shower core [23]. In the same way, comparisons with other kind of detectors have been performed, (spark chamber [24], Geiger counter [25], neon flash tube [26], as well as with thin and thick scintillators [27][28]). But, up to now, there are not exact estimation of the photon contribution. In the energy range $10^5 - 10^7$ GeV all these investigations show both a smooth rise and a noticeable decrease of the photon contribution to the measured shower size versus the distance to the shower core up to 100 m .

Recently the methodical experiment on the MAKET-ANI installation on the Mt. Aragats has been carried out [29]. Comparing the densities measured by scintillators with different thicknesses (1.0 , 1.5 and 5.0 cm), up to 100 m , the ratio $K_\gamma(r)$ of the measured density $\rho_{sc}(r)$ to the charged one $\rho_{ch}(r)$ is described by $K_\gamma(r) = \rho_{sc}(r)/\rho_{ch}(r) = (r/R_M)^{-0.18}$, where r is the distance from the shower core and $R_M = 120\text{ m}$ is the Moliere radius for the observation level of 700 g.cm^2 . According to this result the photon contribution to the charged particle density is $\sim 17\%$ at 50 m from the shower axis and practically disappears at 100 m .

At the same time, simulations show [30][31] a significant increase of the ratio of the photon number to electrons one versus r . Calculations for the real conditions of the GAMMA installation have been performed taking into account the absorber and scintillator thicknesses [32]. According to this work the photon contribution to the measured number of the charged particles is practically constant from 5 to 100 m and is $K_\gamma \simeq 1.25$. The processing of the GAMMA data considering these two results, $K_\gamma(r) = (r/R_M)^{-0.18}$ and $K_\gamma = 1.25$, [29][32], has been made to study the influence of this factor on the measured EAS features.

In *figures 4* the experimental electron lateral distributions are shown for three EAS average size intervals $< N_e > = 2.3 * 10^5$, $7.3 * 10^5$ and $22.8 * 10^5$ as estimated for the two cases of the photon contribution. It can be seen that

in both cases the electron lateral distribution can be very well approximated using the NKG function, but because of the different shape of K_γ versus r , the average age parameter value $\langle S \rangle$ is different by about 0.16.

The comparison between the measured and simulated electron lateral distributions is shown in *figure 5* for the same values of $\langle N_e \rangle$. It can be seen a good agreement for the correction factor $K_\gamma = 1.25 = \text{const.}$ This agreement improves with the increasing of $\langle N_e \rangle$.

It has to be noticed that the age parameter only describes the shape of the charged particles lateral distribution and its values $\langle S \rangle < 1$ do not contradict to the fact that the shower is over the longitudinal development maximum. *Figure 6* shows the dependence of the age parameter $\langle S \rangle$ versus the shower size $\langle N_e \rangle$ from our experimental data processed with $K_\gamma(r) = (r/R_M)^{-0.18}$ and $K_\gamma = 1.25$ and the results from our simulation and the Tien-Shan experimental data [33]. For $\langle N_e \rangle \geq (3 - 5) \cdot 10^5$, experimental data with $K_\gamma = 1.25$ are in a good agreement with the simulation results which is not at all the same in the case of $K_\gamma(r) = (r/R_M)^{-0.18}$ for which the disagreement is large.

For the both variants of processing, the differential size spectra are shown in *figure 7a* for showers in the zenith angle interval $\theta \leq 30^\circ$, (mean atmospheric depth : 738 g.cm^{-2}). In both cases the *knee* can be easily observed. Spectra are approximated in the whole N_e interval by formula [32]: $I(N_e) = A \cdot N_e^{-\gamma_1} (1 + (N_e/N_e^{\text{knee}})^k)^{-(\gamma_1 - \gamma_2)/k}$. The spectra differ mainly at the beginning and the end of the size interval, (by no more than 20%). Spectral indexes difference for GAMMA for both cases is $\Delta\gamma = 0.36 \pm 0.02$. The *knee* regions approximately coincide at $N_e^{\text{knee}} \approx (1.8 - 2.0) \cdot 10^6$. The integral intensity for the range of $N_e \geq N_e^{\text{knee}}$ is $(1.3 \pm 0.4) \cdot 10^{-7} \text{ m}^{-2} \text{ s}^{-1} \text{ sr}^{-1}$. This result is in agreement with the data of other experiments [34][35].

In order to demonstrate the *knee* region properties more visually spectra are given in *figure 7b* multiplied by $N_e^{2.5}$. For the case of $K_\gamma = 1.25$ spectral index is less by (0.07 ± 0.02) in the whole N_e region.

In the *figure 8*, the size spectra for the two zenith angle intervals are shown at $\langle \theta \rangle = 14^\circ$ and $\langle \theta \rangle = 31^\circ$ to make the qualitative assessment of the behaviour of the spectra at different angles. They are practically parallel and coincide when data with $\langle \theta \rangle = 31^\circ$ are shifted. Such behaviour corresponds to the shower absorption length of $\Lambda = (230 \pm 25) \text{ g} \cdot \text{cm}^{-2}$ below the knee and $(230 \pm 40) \text{ g} \cdot \text{cm}^{-2}$ above up to $N_e = 5 \cdot 10^6$. The permanency of the attenuation length is one evidence of the constant charged particle

composition of the showers below and above the *knee* only and says nothing about the cause of the *knee*.

In *figure 9* the spectra are shown with various cuts of the age parameter S . Relatively *old* shower spectrum ($S > 0.85$) practically has no *knee* and is steeper than all shower spectrum. On the other hand, the *young* shower spectrum ($S < 0.75$) has the obvious *knee* and is flatter, than the all shower spectrum below the *knee* and is almost parallel to it above. These spectra may be explained with both hypotheses of the *knee* origin noted in the introduction, because of the region of $N_e \geq (1 - 2) \cdot 10^6$ is transitional. The *young* showers fraction does not arise above the *knee* because of change of the mass composition to heavier one in the model of primary *knee*. In the case of change of the hadron interaction the fraction of the heavy-like events will rise among the showers generated by primary protons.

3.2 Muon component characteristics

As it was mentioned above, the underground muon detectors are placed in the hall and tunnel of the GAMMA underground part. Due to the different shieldings of concrete, iron and ground above detectors, muons with two energy thresholds $E_\mu \geq 5 \text{ GeV}$ (hall) and $E_\mu \geq 2.5 \text{ GeV}$ (tunnel) are detected. The muon lateral distributions for given thresholds and three $\langle N_e \rangle$ intervals are shown in *figure 10 a*. These distributions are limited by the number of detectors and their disposition in the hall and tunnel. Moreover, close to the shower core the signal in the detectors are strongly affected by the contribution of other type of particles due to the punch through effect. So, the correct determination of the muon lateral distribution is available at distances $[8 - 52] \text{ m}$ for $E_\mu \geq 5 \text{ GeV}$ and $[20 - 90] \text{ m}$ for $E_\mu \geq 2.5 \text{ GeV}$. In the interval of $[0 - 50] \text{ m}$, the shapes of lateral distribution are very similar for the both muon energy thresholds. This gives the possibility to find a transition coefficient from the density of muons with $E_\mu \geq 2.5 \text{ GeV}$ to the muon density with $E_\mu \geq 5 \text{ GeV}$, which is $\rho(2.5 \text{ GeV})/\rho(5 \text{ GeV}) \approx 1.35$, for all $\langle N_e \rangle$ intervals. In *figure 10 b*, the muon lateral distribution with the energy threshold $E_\mu \geq 5 \text{ GeV}$ for the hall detectors and reconstructed one from the distribution of tunnel detectors are presented. These distributions are well approximated by the Hillas function, [36], $\rho_\mu(N_e, r) = 0.9 (N_e/10^5) r^{-(0.75+0.06 \cdot \ln(N_e/10^5))} \exp(-r/80)$. This formula describes well the experimental data for $N_e < 2 \cdot 10^6$. Farther, the dependence of ρ_μ versus

N_e becomes stronger but the shape of the distribution remains the same.

The approximations of the Tien-Shan data [37], for the same energy threshold $E_\mu \geq 5 \text{ GeV}$ and the same observation level $700 \text{ g} \cdot \text{cm}^{-2}$ are presented by $\rho_\mu(N_e, r) = 0.95 (N_e/10^5)^{0.8} r^{-0.75} \exp(-r/80)$. This formula describes the GAMMA experimental data noticeably worse, especially for $N_e > 10^6$.

As it was mentioned above, the lateral distribution of muons in our experiment, ($E_\mu \geq 5 \text{ GeV}$), is studied for distances $r \leq 52 \text{ m}$ from the shower core where about 33% of all muons are contained. Obtaining the total muon number, N_μ , by integration the muon lateral distribution function, the possible extrapolation errors for $r > 52 \text{ m}$ will give an error in the N_μ estimation. On the other hand, closer to the shower axis, $r \lesssim 8 \text{ m}$, other kinds of particles give a considerable contribution to muon lateral distribution. For this reason, we use the truncated muon number, N_μ^{trun} , which is the number of muons in the ring $8 \text{ m} < r < 52 \text{ m}$. Experimentally, the truncated muon number is determined as $N_\mu^{trun}(r) = \sum (\rho_i^{ex} / w_\mu^{trun}(r)) / K$, where:

K is number of detectors in the given interval of r ;

ρ_i^{ex} is the experimental muon density in the i^{th} detector and

$w_\mu^{trun}(r)$ is the truncated muon probability distribution, determined by our muon lateral distribution approximation.

It should be noticed, that according to simulations, $N_\mu^{trun}(>5 \text{ GeV})$ in our experiment depends on the primary particle mass. *Figure 11* shows N_μ^{trun} dependence on N_e . Up to $N_e \approx 2 \cdot 10^6$ it can be fitted with the expression $N_\mu^{trun} \sim N_e^{0.79}$. For larger N_e dependence becomes steeper. It should be noted that because of the shower size threshold $N_e > 10^5$ the registration of the shower with fixed muon size and 100% efficiency is possible at $N_\mu^{trun} \gtrsim 10^3$.

The differential N_μ^{trun} spectrum is plotted on *figure 12*. It can be seen that there is no obvious *knee*, but the data do not contradict to change of spectral index by (0.1-0.2) at $N_\mu^{trun} > 5 \cdot 10^3$. Contrary to the case of fixed N_e the showers at fixed N_μ are enriched by the showers generated by heavy primaries. If the proton spectrum has a *knee* only then the N_μ spectrum will have feebly marked *knee*. At energies above the possible *knee* position of the primary iron spectrum, N_μ spectrum will obtain the final index different by $\Delta\gamma \approx 0.5$ from present one. It is necessary to expand our measurements to this energy region.

Situation in the case of the change of hadron interactions for sufficiently high energies depends on details of the secondary spectra but the difference

of indexes will be not bigger.

In order to interpret our experimental results the instrumental response has to be taken into account. For this purpose the detector simulation program ARES (ARagats Events Simulation) [38] based on the GEANT package.[39] has been developed for the GAMMA installation. The data from CORSIKA simulated EAS are used as input for the ARES code.

To take into account the detector response to EAS muon component all secondary particles of EAS at the ground level are passed through the absorber and muon detectors. For each shower the deposited energy and the muon number in the individual detector are obtained (the methodical procedure of muon number estimation is described in [40][41]). The muon lateral distribution are derived using the CORSIKA simulation data in the primary energy range of $3 \cdot 10^5$ - 10^7 GeV for the different primary groups. *Figure 13 (a, b)* shows the muon lateral distributions in the shower size range $1.78 \cdot 10^5 < N_e < 3.16 \cdot 10^5$ in the case of the normal mixed composition for the tunnel and hall detectors. The experimental distribution and the CORSIKA/ARES simulation results (with the corresponding muon thresholds) are in a good agreement.

4 Conclusions

The study of the EAS electrons and muons ($E_\mu > 5$ GeV and $E_\mu > 2.5$ GeV) by the GAMMA array gives reliable information about EAS characteristics in the shower size range of 10^5 - 10^7 . There are not noticeable contradictions of our data with other experiments. Using the contribution of the EAS gamma-quanta equal $K_\gamma = 1.25 = const$ an agreement between CORSIKA simulation and experimental data is obtained.

Permanency of the age parameter S at $N_e > 2 \cdot 10^6$ and steepening of N_μ^{trun} depending on N_e at the same range by N_e conform to the more rapid shower development. The data in the shower size interval $N_e^{knee} \div 10 \cdot N_e^{knee}$ are not decisive for the problem of the *knee* origin and enlargement of the study range is necessary for the complex installations to make sure conclusion about the primary composition and spectra. With the object to extend a possibilities of the GAMMA installation it is expected to decrease the registration threshold by N_e and to enlarge an effective area of the shower selection with $N_e > 10^6$.

The present paper is based on the ANI collaboration data bank and express the point of view of the given group of co-authors.

4.1 Acknowledgments

The present investigations are embedded in a collaboration between the Moscow Lebedev Institute (Russia), the Yerevan Physics Institute (Armenia) and the Universite de Bordeaux 1 (France).

We give thanks to the Staff of the Aragats Research Station for the assistance during the longterm maintenance of the GAMMA installation.

We are grateful to all colleagues of the Moscow Lebedev Institute who were taking part in the development and creation of the GAMMA installation. We would like to express our special gratitude to N.M. Nikolskaya for the creation of the software and to prof. S.I. Nikolsky for useful discussions.

We thank also prof. S. Ter-Antonyan and E.Mnatsakanyan for some useful remarks and comments and we do not forget P. Aguer from the CENBG, (CNRS-In2p3-France) whose help has been useful.

This work was supported by the grant 96-752 of the Armenian Ministry of Industry, by the Russian RFBR 96-02-18098 grant and by the Russian Energy Ministry.

5 Figures

Figure 1. Layout of the GAMMA installation

Figure 2. Schematic view of the muon underground detector

Figure 3. Muon lateral distributions at the different azimuth angles φ :

a) hall, b) tunnel

Figure 4. Electron lateral distributions for two cases of the photon contribution

a) $K_\gamma(r) = (r/R_M)^{-0.18}$, b) $K_\gamma(r) = 1.25 = const$

Figure 5. Electron lateral distribution in comparison with the CORSIKA simulation for two cases of the photon contribution

Figure 6. The average age parameter $\langle S \rangle$ versus shower size $\langle N_e \rangle$ at two cases of the photon contribution in comparison with CORSIKA simulation and Tien-Shan data

Figure 7. Differential size spectra at two cases of the photon contribution

Figure 8. Differential size spectra at different zenith angles

Figure 9. Differential size spectra at different interval by age parameter

Figure 10. Muon lateral distribution at different shower sizes in

a) hall, b) tunnel

Figure 11. Average truncated muon number $\langle N_{\mu}^{tun} \rangle$ versus number of electrons $\langle N_e \rangle$

Figure 12. Differential spectrum of truncated muon number

Figure 13. Muon lateral distributions in comparison with CORSIKA and ARES simulation results:

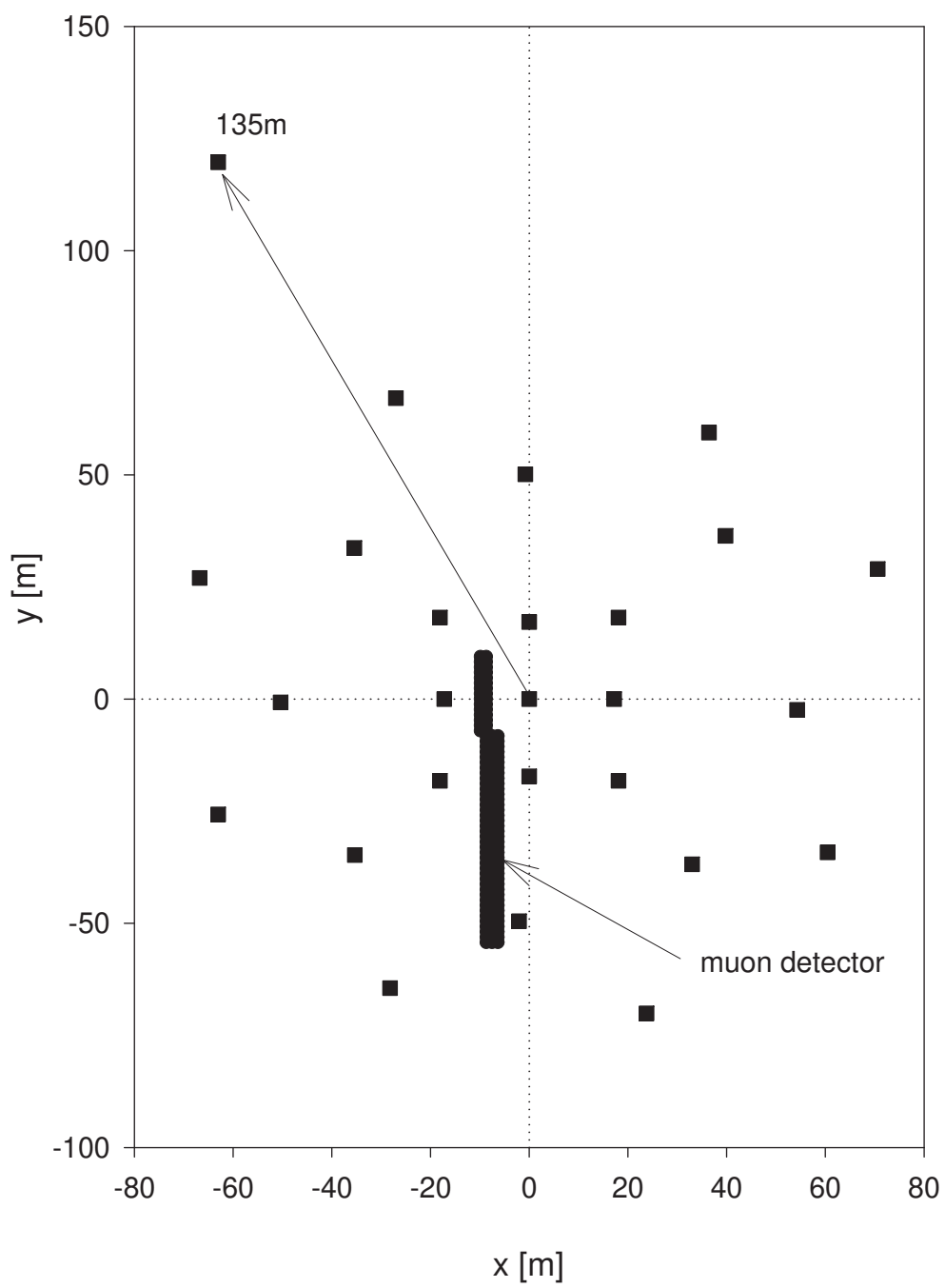
a) hall, b) tunnel

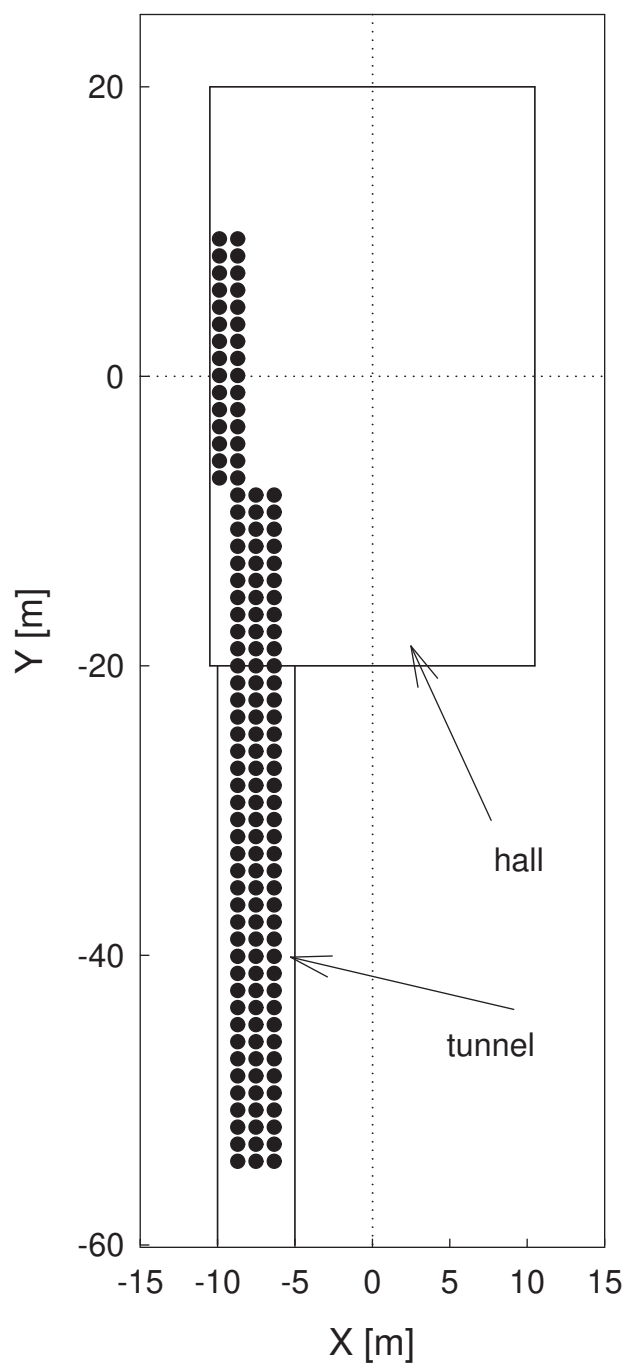
References

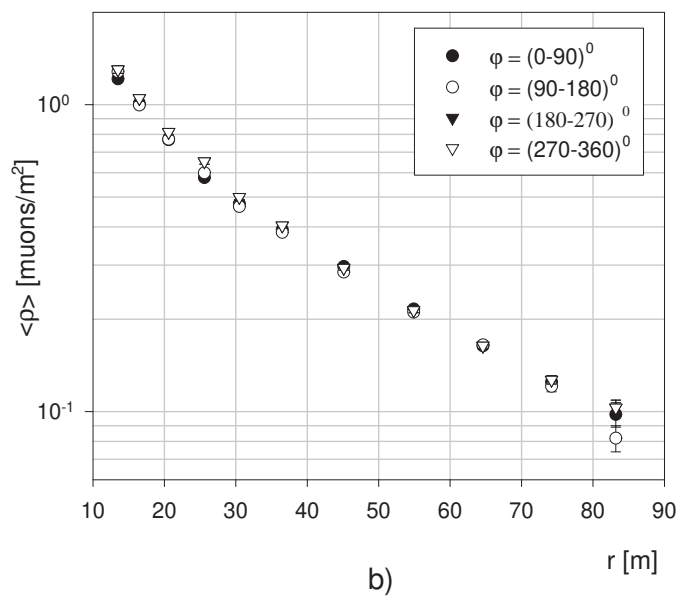
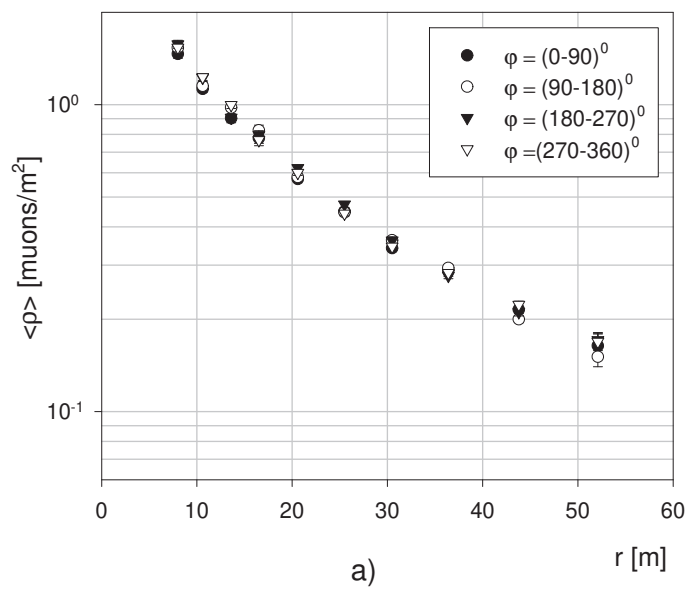
- [1] G.V. Kulikov and G.B. Khristiansen, 1958, *JETP*, **35**, 635
- [2] P.R. Blake and W.F. Nash, 1998, *J.Phys.G:Nucl.Part.Phys.*, **24**, 217
- [3] Yu A Fomin, N.N. Kalmykov, G.B. Christiansen, G.V. Kulikov, V.I.Nazarov, S.S. Ostapchenko, A.I. Pavlov, V.I. Solovjeva, V.P. Sulakov, A.V. Trubitsyn and E.A. Vishnevskaya, 1996, *J. Phys. G:Nucl. Part. Phys.*, **22**, 1839
- [4] W Rhode *et al.*, 1996, *Nucl. Phys.B,Proc. Suppl.*, **48**, 491
- [5] M. Roth *et al.*, 1999, *Proc. 26th International Cosmic Rays Conference*, Salt Lake City, **1**, 333
- [6] J. Engler *et al.*, 1999, *Proc. 26th International Cosmic Rays Conference*, Salt Lake City, **1**, 349
- [7] M.A.K. Glasmacher, *et al.*, 1999, to appear in *Astro. Phys.* 1999, *Proc. 26th International Cosmic Rays Conference*, Salt Lake City, **3**, 129
- [8] S.I. Nikolsky, 1995, *Nuclear Physics B*, **39A**, 228
- [9] S.I. Nikolsky, 1999, *26th International Cosmic Rays Conference*, Salt Lake City, **1**, 59
- [10] D.S. Adamov *et al.*, 1991, *Izv.A.N.SSSR., ser. phys.*, **55**, 4, 703
- [11] H.O .Klages *et al.*, 1997, *Nucl. Phys.B,Proc. Suppl.*, **52B**, 92
- [12] L.D. Vildanova *et al.*, 1994, *Izv.A.N.SSSR., ser. phys.*, **58**, 12, 79

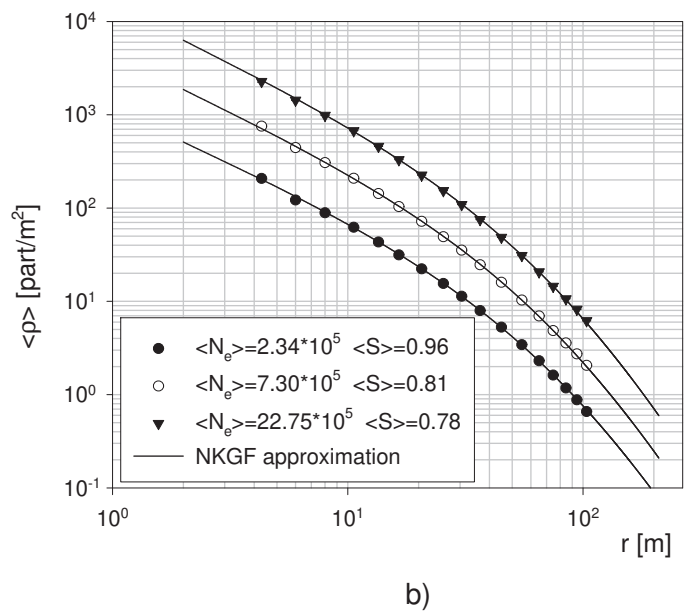
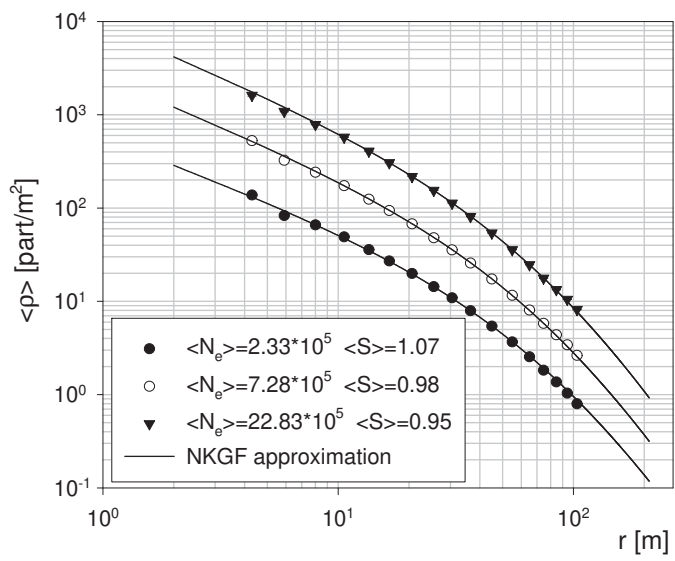
- [13] Yu A Fomin, N.N *et al.*, 1991, *Proc. 22th International Cosmic Rays Conference*, Dublin, **2**, 85
- [14] M. Aglietta *et al.*, 1993, *Nuclear Instruments & Methods*, **A420**,117
- [15] A. Barione *et al.*, 1994, *Nuclear Instruments & Methods*, **A346**,329
- [16] D. Heck, J. Knapp, J.N. Capdevielle, G. Schatz, T. Thouw, 1998, *ForschungszentrumKarlsruhe*, FZKA 6019
- [17] 1993, *Phys. Rep.*, **232**, 87
- [18] S.A. Arzumanian *et al.*, 1995, 24th *International Cosmic Rays Conference*, Roma, **1**,482
- [19] T.V. Danilova *et al.* 1983, *Proc. 18th International Cosmic Rays Conference*, Bangalore, **8**, 104
- [20] E.A.Mnatsakanyan, 1999, *Preprint YerPhI*, 1545(19)-99
- [21] V.S. Aseikin, N.M.Nikolskaya, V.P Pavlyuchenko, E.I.Tukish., 1987, Moscow, *P.N.Lebedev Institute*, Preprint No 31
- [22] V.P.Pavlyuchenko, 1981, *Moscow, P.N.Lebedev Institute*, Report 8
- [23] C. Wallace, 1960,*Proc. 20th International Cosmic Rays Conference*, (in Russia), Moscow, **2**, 334
- [24] S. Shibata *et al.*, 1965, *Proc. 9th International Cosmic Rays Conference*, London, **2**, 672
- [25] A.E. Chudakov *et al.*, 1979, 16th *International Cosmic Rays Conference*, Kyoto, **8**, 217
- [26] E.R. Bagge, M. Samorski, W. Stamm, 1979, 16th *International Cosmic Rays Conference*, Kyoto, **13**, 260
- [27] T. Hara *et al.*, 1979, 16th *International Cosmic Rays Conference*, Kyoto, **13**, 148
- [28] K.Asakimori *et al.*, 1979, 16th *International Cosmic Rays Conference*, Kyoto, **8**, 252

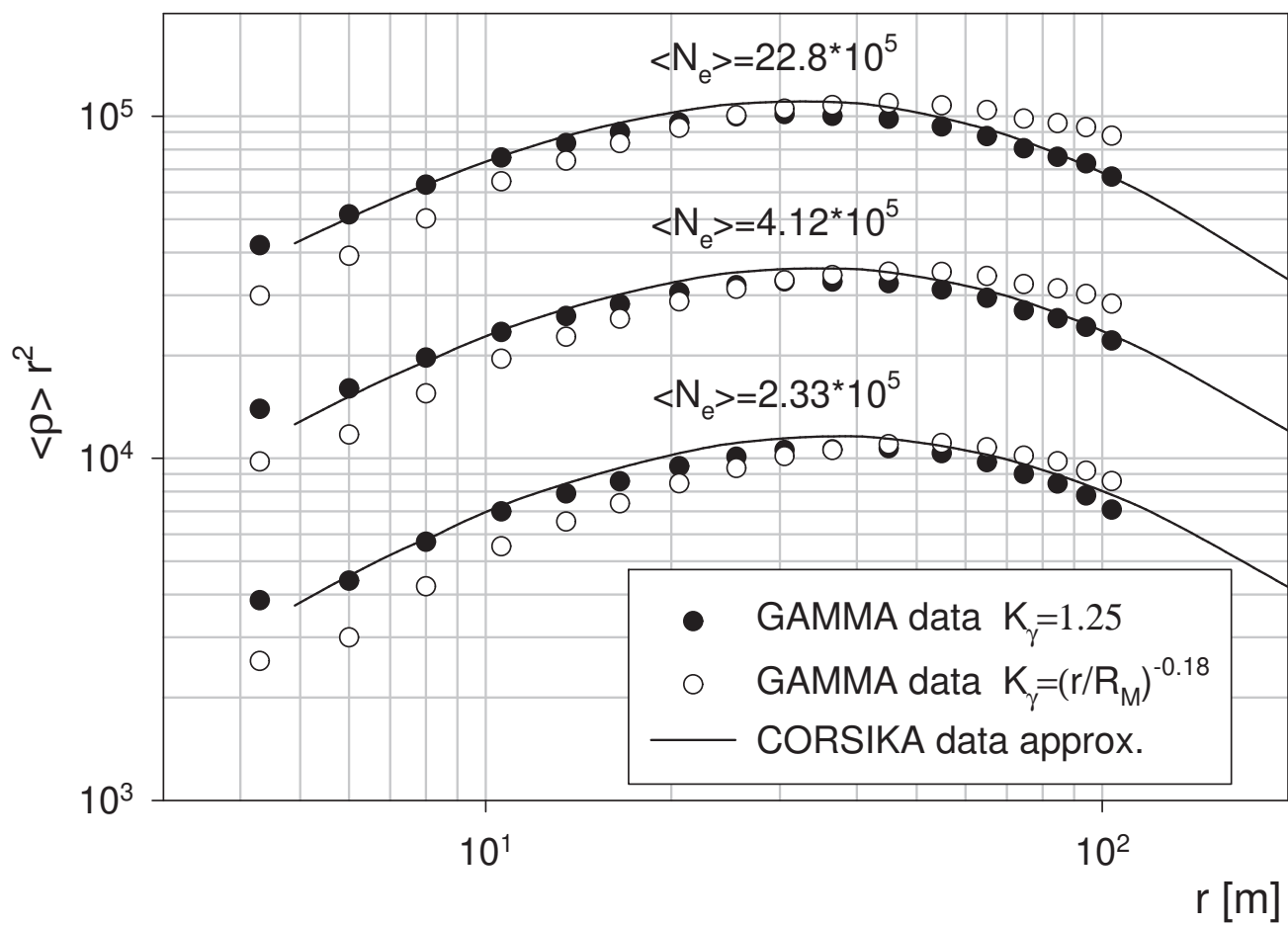
- [29] S.V. Blokhin, V.A. Romakhin, G.G. Hovsepyan, 1999, *Proc. of the Workshop ANI-99*, to be printed
- [30] J.H. Weber, 1997, *Proc. 25th International Cosmic Rays Conference*, Durban, **6**, 153
- [31] K. Sanosyan, 1999, *Proc. of the Workshop ANI-99*, to be printed
- [32] S.V. Ter-Antonyan, 1998, *Private communication on Workshop ANI-98*
- [33] D.S. Adamov, 1990, *Dissertation*, FIAN, Moscow
- [34] G. Navarra, 1998, *Nucl. Phys. B (Proc. Suppl.)*, **60B**, 105
- [35] H.Rebel, 1998, *Proc. of the Workshop ANI-98*
- [36] A.M .Hillas *et al.*, 1969, 16th *International Cosmic Rays Conference*, Budapest, **3**, 533
- [37] V.S.Aseikin *et al.*, 1979, *Moscow, P.N.Lebedev Institute*, Report 109, 3
- [38] A .Haungs, A.F. Badea, M.Z. Zazyan, *Proc. of the Workshop ANI-99*, to be printed.
- [39] GEANT: *CERN Program Library Long Writeup*, W5013, CERN (1993).
- [40] M.Z. Zazyan, A. Haungs, *Proc.of the Workshop ANI-98*, FZKA 6215, Forshungszentrum Karlsruhe, 1998, p.37.
- [41] M.Z.Zazyan *et al.*, *Proc. of the Workshop ANI-99*, to be printed

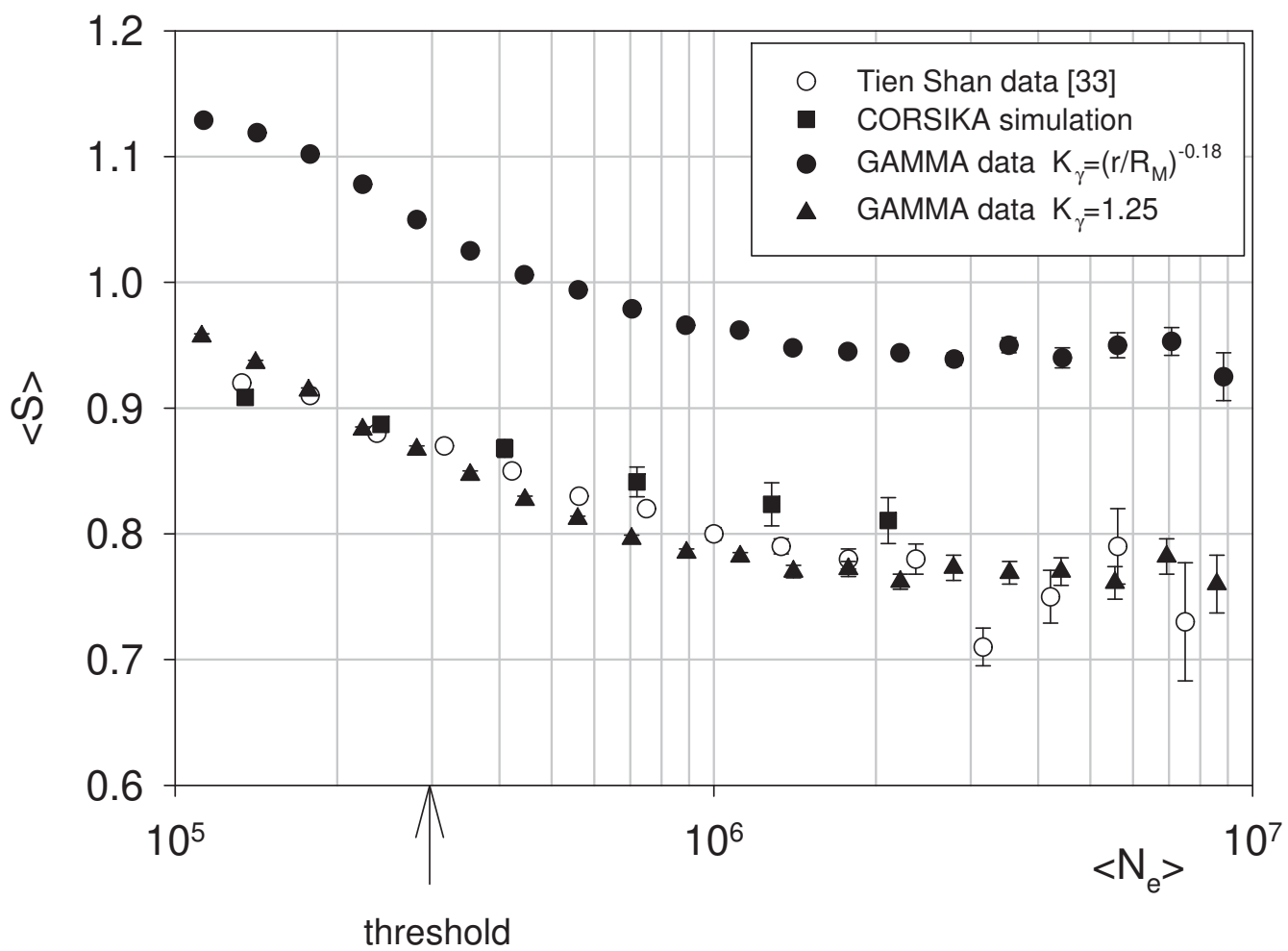


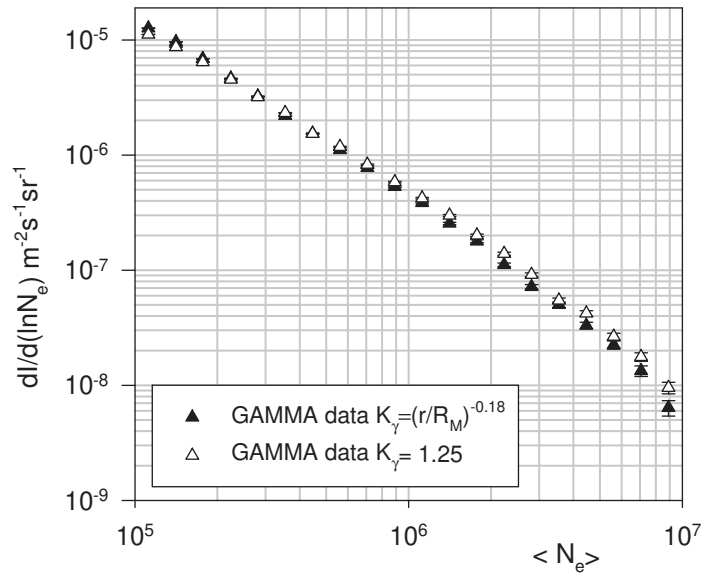




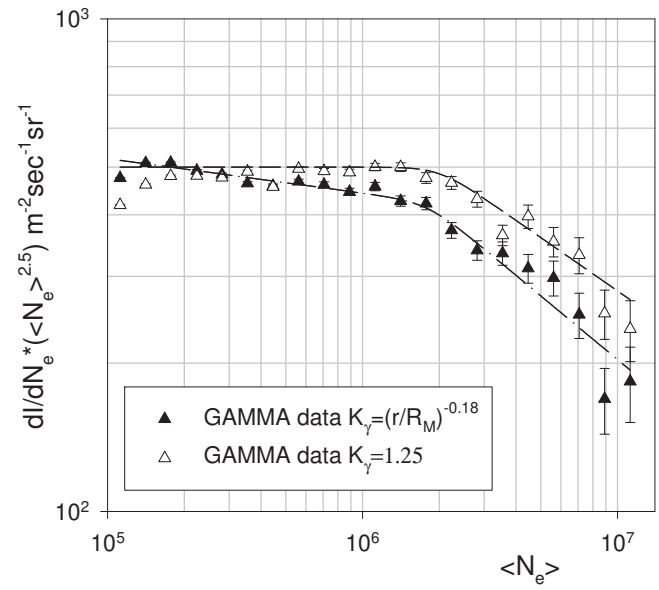




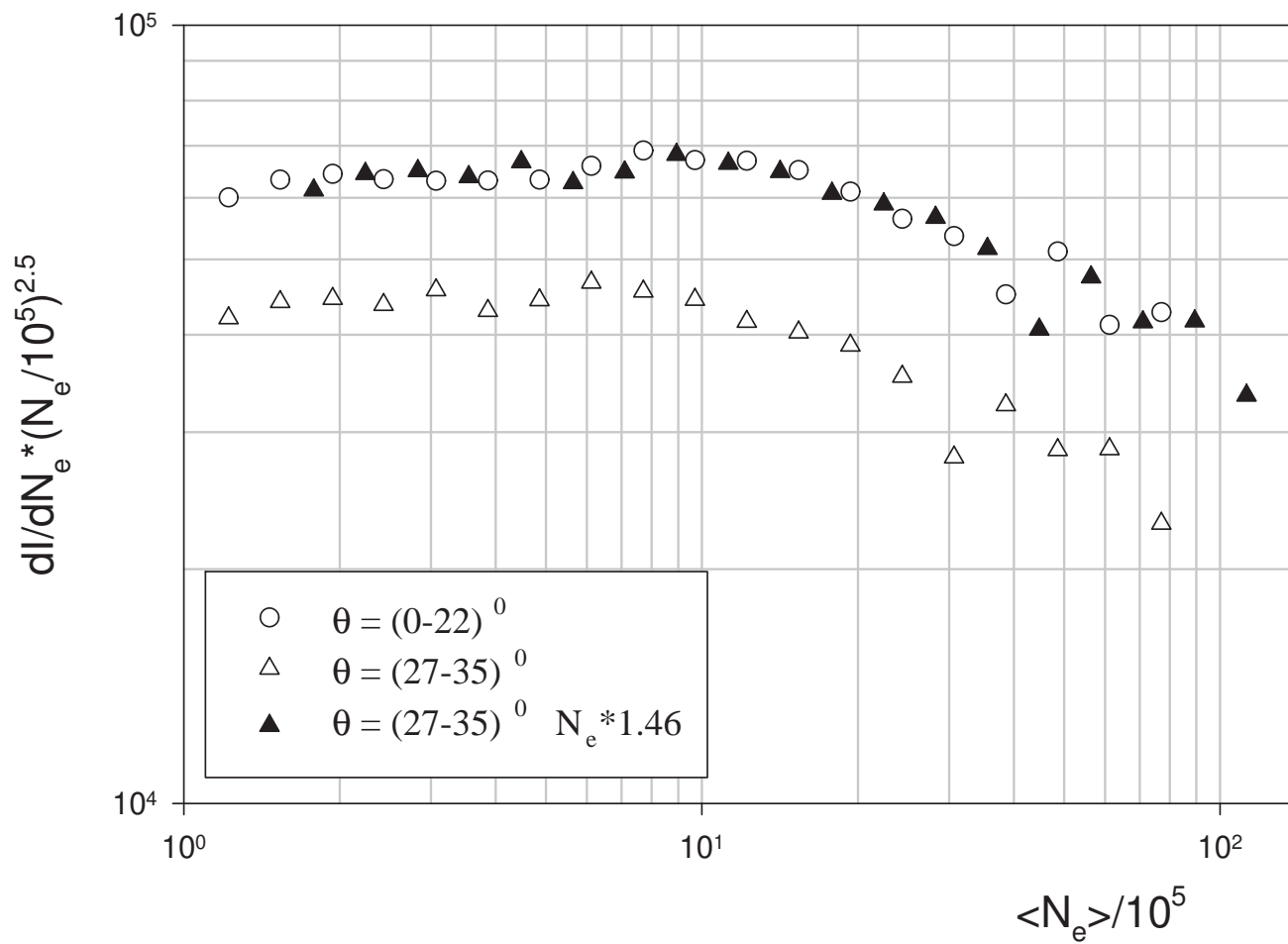


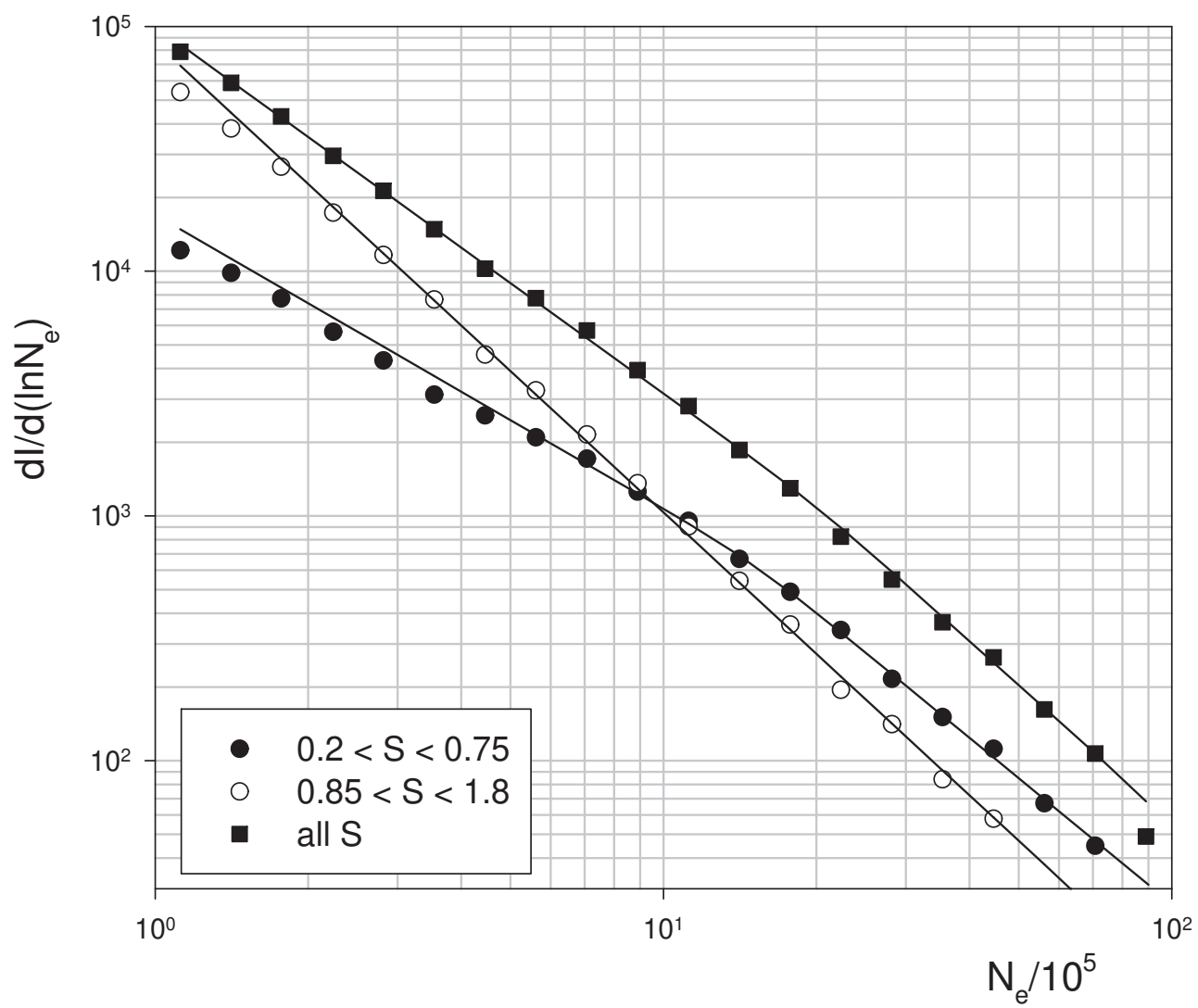


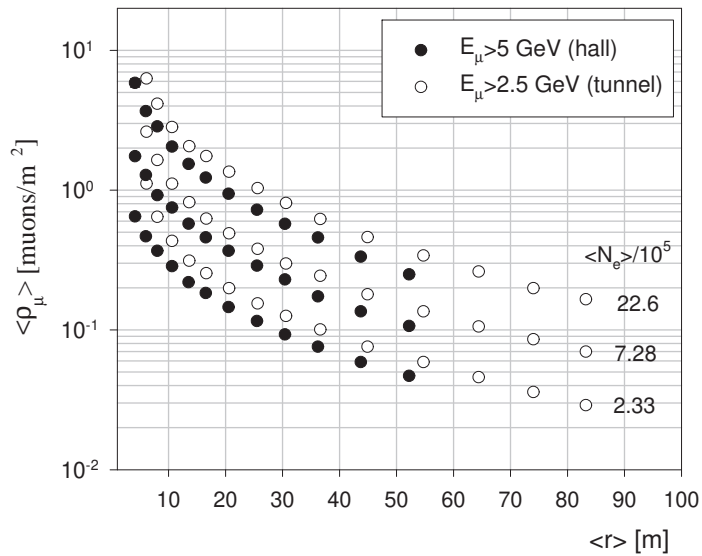
a)



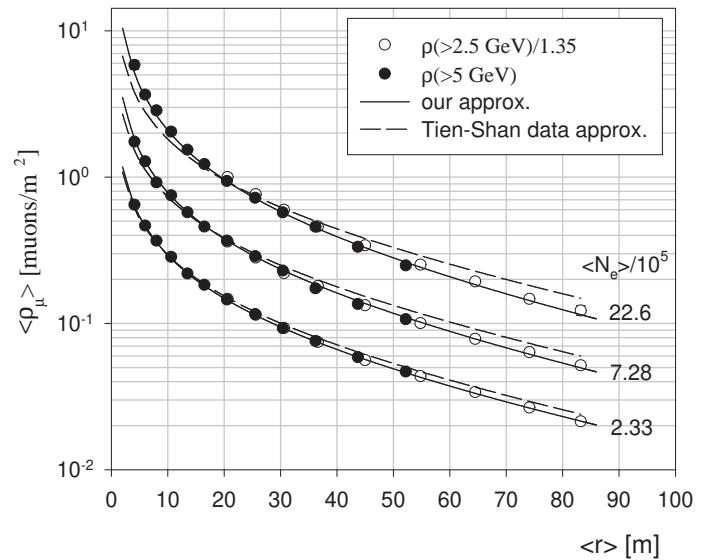
b)



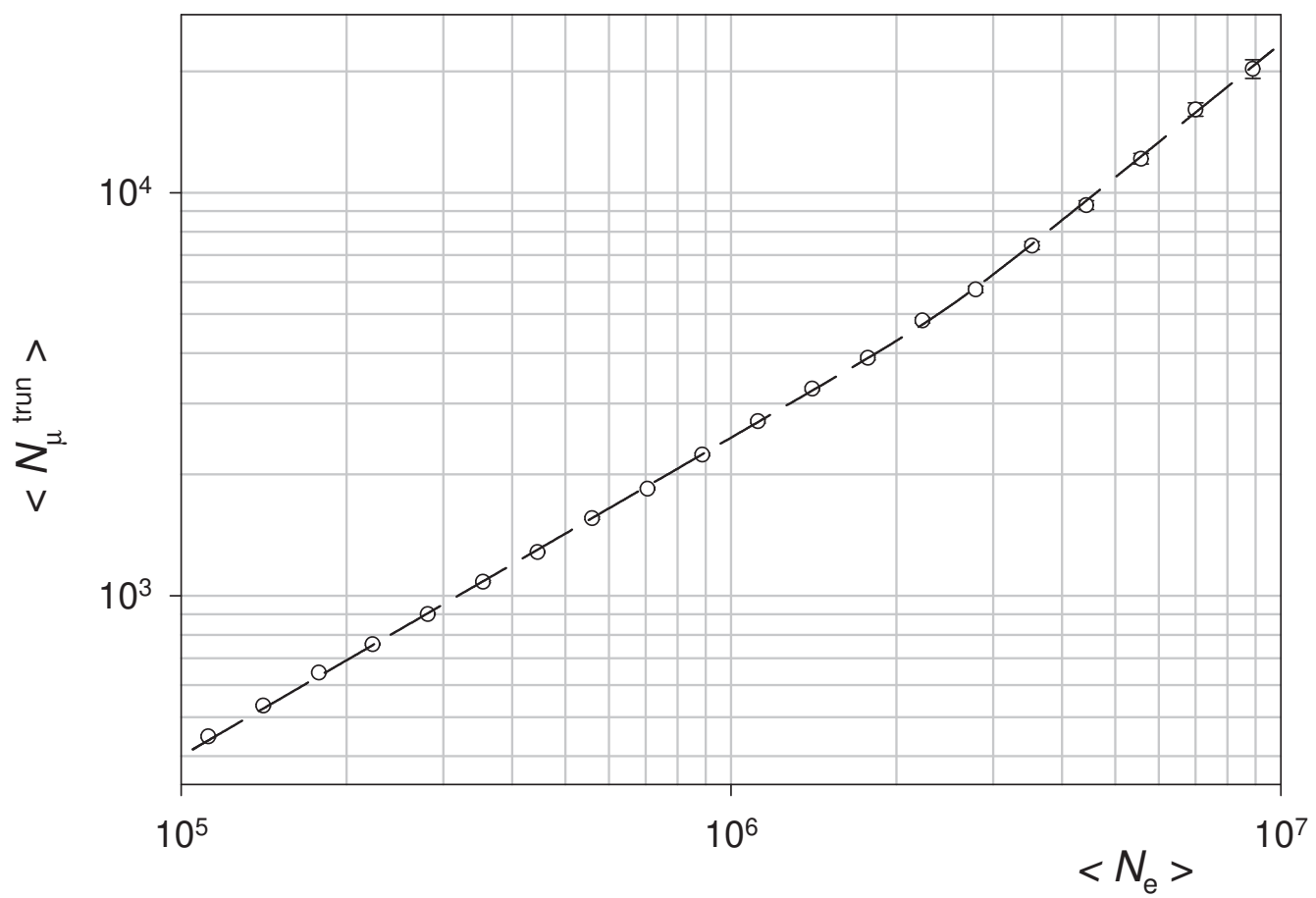


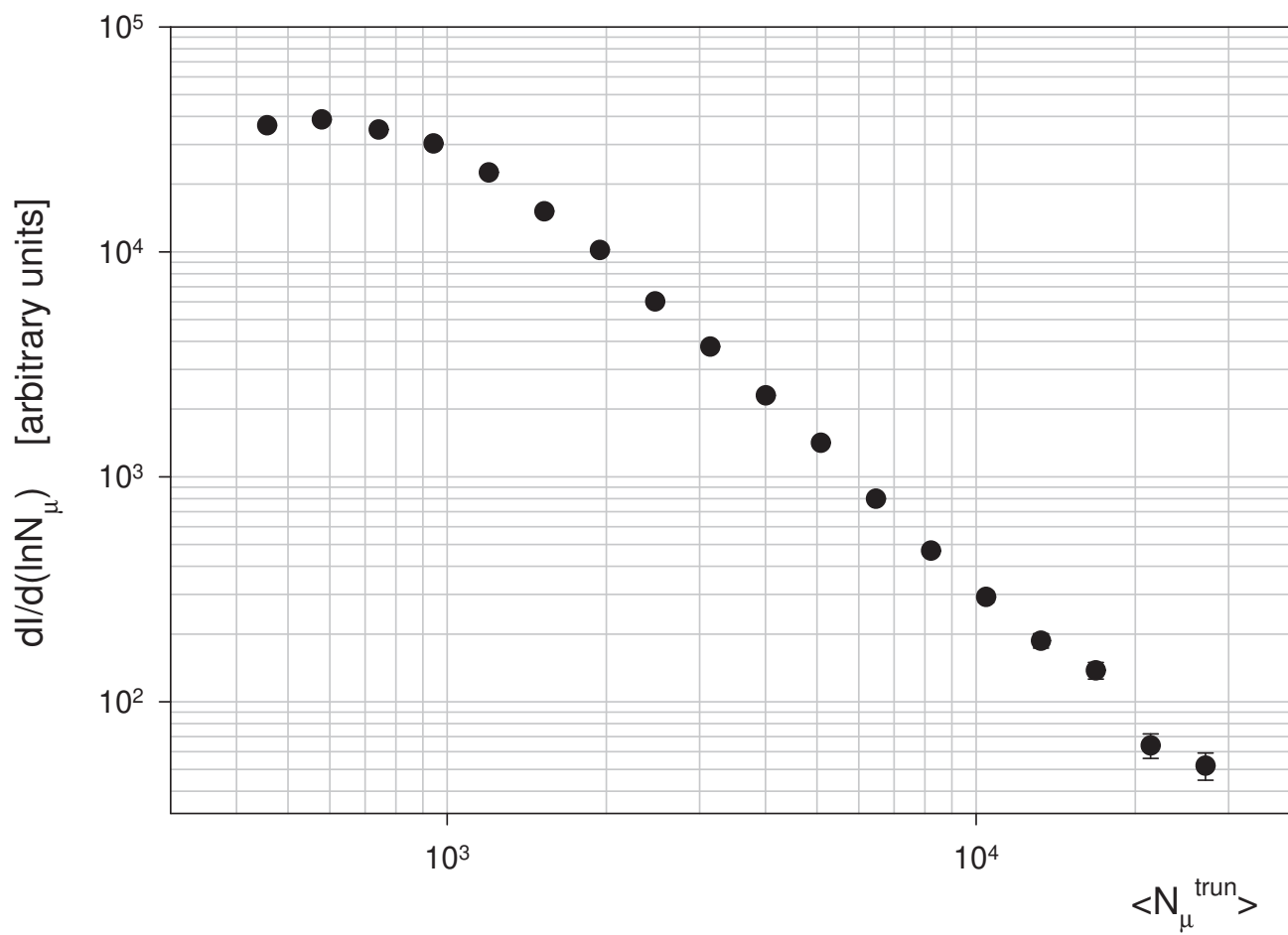


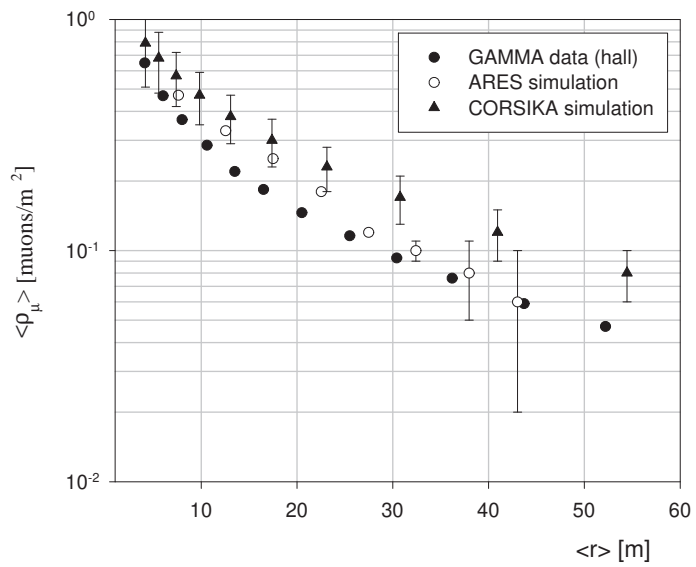
a)



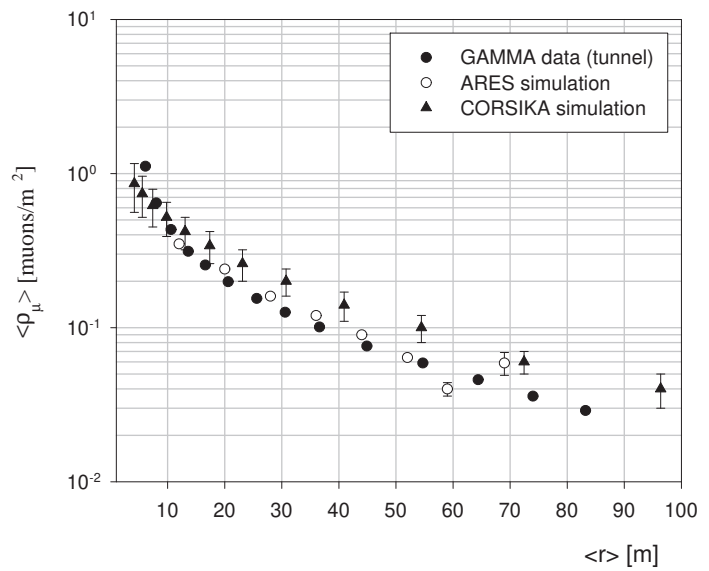
b)







a)



b)